Int J Multiphase Flow Vol 18, No 1, pp 89–101, 1992
Printed in Great Britain

0301-9322/92 $5.00 + 0.00

AN INTEGRAL SHEAR LAYER METHOD FOR THE NUMERICAL PREDICTION OF STEAM–DROPLET FLOWS

CH. MALAMATENIOS, K. GIANNAKOGLOU and K. D. PAPAILIOU
Laboratory of Thermal Turbomachines, National Technical University of Athens, P.O Box 64069, 15710 Athens, Greece

(Received 11 November 1990; in revised form 15 July 1991)

Abstract—A complete two-phase shear layer calculation method is presented for the prediction of non-equilibrium effects occurring in the vicinity of solid walls. Water droplets are treated in a Lagrangian fashion and an integral shear layer technique, capable of handling both attached and separated compressible shear layers, is used for the carrier phase. A parametric analysis concerning the most representative shear layer quantities is included in detail. A number of theoretical test cases are investigated including single- and two-phase flows, under different inlet droplet conditions, in a two-dimensional convergent–divergent duct.

Key Words: two-phase flow, shear layer, turbulent flow, Lagrangian approach

1. INTRODUCTION

Low efficiency and blade erosion are the two main problems associated with wetness in steam turbines, employed in large-scale electricity generation. Nowadays, due to increasing fuel costs, it has become particularly important to optimize the performance of these machines, not only for minimum aerodynamic loss but also for minimum wetness loss.

Over the last few decades, it has been common design practice to predict the wetness loss using empirical rules. More recently, theoretical approaches have been developed based on the application of the one-dimensional wet steam theory to the turbine geometry. However, the flow pattern in a low-pressure turbine stage with a twisted blading is strongly three-dimensional. The simple one-dimensional approach is, therefore, of little value and, in order to provide a useful design tool, the researcher must adapt his theory for use with conventional turbomachinery calculation methods.

For the complex turbulent flows encountered in turbine blade passages, an acceptable way of circumventing the time-comsuming task of solving the full Navier–Stokes equations, without losing too much accuracy, is to use the two-zone hypothesis, which is based on the decomposition of the flow into an inviscid and a viscous part. Consequently, two different computing tools are necessary, one that deals with the viscous effects and another that deals with the inviscid external flow (Malamatenios *et al.* 1990). The two-zone hypothesis is employed here, where the flow, presented schematically in figure 1, is considered as purely two-dimensional.

The objective of the present paper is to present in detail the theoretical aspects upon which a complete two-phase shear layer integral calculation method was built. The authors do not intend to further analyse either the external two-phase solver or the coupling techniques related to the two-zone approach, since this was the subject of the abovementioned publication. An existing single-phase integral shear layer method, which has been extensively validated in a variety of cases (Papailiou & Bouras 1990; Bouras 1991; Papailiou 1981), was used as a basis for the development of the two-phase method. All the necessary modifications to the existing single-phase method, as well as the differences and similarities between all the involved quantities, are presented and discussed in the following paragraphs.

In order to simulate the motion of the droplets within the shear layer, the Lagrangian approach was used and the dispersed phase was regarded as a source of mass, momentum and energy to the

continuous one, as proposed by Crowe *et al.* (1977). It is an identical approach to the one incorporated in the external flow region solver for the treatment of the particulate phase. The method allows for a flux of droplets entering or exiting the shear layer boundary; this flux may be calculated once the communication between the core flow and the shear layer has been established.

2. THEORETICAL ANALYSIS AND METHOD OF SOLUTION

For the sake of completeness, a few words about the two-zone approach are in order. In the vicinity of the wall, the presence of the shear layer retards the flow, displacing the outer flow streamlines (blockage effect). The outer flow therefore "sees" an effective body which is thicker than the real one by the displacement thickness. The overall calculation is carried out in an iterative manner, each inviscid solution providing the external flow conditions for the following shear layer calculation, while the shear layer solution provides boundary conditions for the following inviscid calculation (Malamatenios *et al.* 1990; Papailiou & Bouras 1990). Iterations continue until convergence. Such an iterative procedure is possible with the present formulation, even if strong separation is present.

The same, essentially, iterative procedure is applied for two-phase flows. In this case, however, boundary conditions for additional quantities have to be specified, in particular the droplet size, temperature and velocity vector at the shear layer edge, along with the void fraction values at the same boundaries. The analysis of the viscous part of the flow constitutes a parabolic problem, which requires the solution of two integral equations for the gaseous phase together with the transport equations for the water droplets, in order to predict the development of the two-phase shear layer along a solid surface.

2.1. Governing equations for steam

The basic equations for steam are expressed in a rotating frame of reference. These are the two-phase local time-averaged equations, introduced by Delhaye (1981). In order to treat the viscous problem on the blade-to-blade surface, the continuity, momentum and energy equations are written in a curvilinear coordinate system (s, n) (see figure 1), where the s-lines of the system coincide with the real flow streamlines. By subtracting the basic equations, as written for the external and the real flow, the corresponding deficit equations are formulated, which are finally integrated along the normal to the streamwise direction (**n**). By introducing the definitions of the

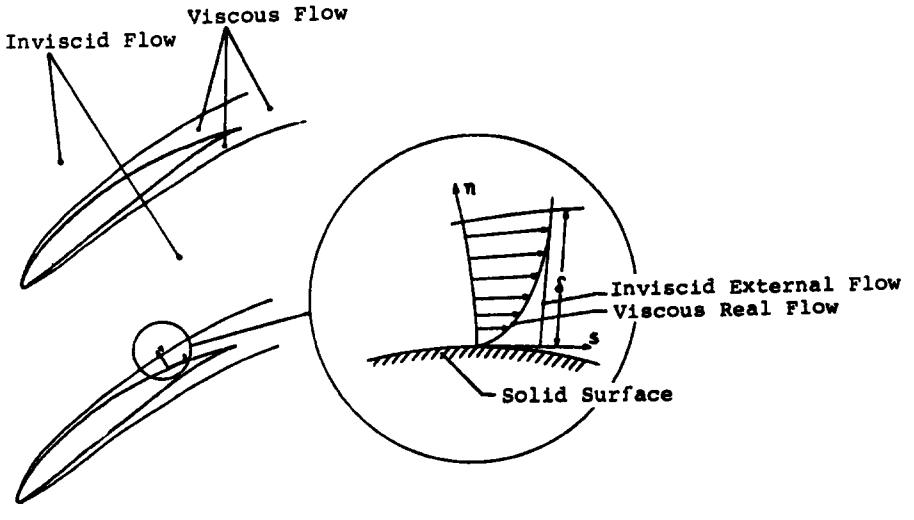

Figure 1 Schematic representation of the two-zone model for a two-dimensional cascade.

various thicknesses and the other integral quantities, as described in appendix A, the following equations are formulated:

(a) the streamwise momentum integral equation,

$$\frac{\mathrm{d}(\sigma\epsilon_{\mathrm{ew}}\rho_{\mathrm{ew}}W_{\mathrm{Sew}}^3\delta_2)}{\sigma\epsilon_{\mathrm{ew}}\rho_{\mathrm{ew}}W_{\mathrm{Sew}}^3\delta_2}+(H_{12}-1)\frac{\mathrm{d}W_{\mathrm{Sew}}}{W_{\mathrm{Sew}}}=\frac{H_{\rho 2}}{W_{\mathrm{Sew}}^2}\mathrm{d}\left(\frac{\Omega^2R^2}{2}\right)+\frac{C_{\mathrm{f}}}{2\delta_2}\mathrm{d}s+A_{\mathrm{m}}+G_{\mathrm{m}}; \quad [1]$$

and

(b) the mean-flow kinetic energy integral equation,

$$\frac{\mathrm{d}(\sigma\epsilon_{\mathrm{ew}}\rho_{\mathrm{ew}}W_{\mathrm{Sew}}^3\delta_3)}{\sigma\epsilon_{\mathrm{ew}}\rho_{\mathrm{ew}}W_{\mathrm{Sew}}^3\delta_3}+r(\gamma-1)M_{\mathrm{ew}}^2\frac{\mathrm{d}W_{\mathrm{Sew}}}{W_{\mathrm{Sew}}}=\frac{r(\gamma-1)M_{\mathrm{ew}}^2}{W_{\mathrm{Sew}}^2}\mathrm{d}\left(\frac{\Omega^2R^2}{2}\right)+\frac{C_{\mathrm{D}}}{\delta_3}\mathrm{d}s+A_{\mathrm{e}}+G_{\mathrm{e}}; \quad [2]$$

where R, Ω, γ and r denote the radius, rotational speed of the machine, ratio of the specific heats of gas and a recovery factor (Papailiou 1981), respectively. In [1] and [2], the terms G_{m} and G_{e} are the source terms that introduce the effect of the dispersed phase to the continuous one, while A_{m} and A_{e} are source terms introducing the influence of the surface curvature and the normal fluctuation terms on the gaseous phase shear layer (Bouras 1991).

During the development of the governing equations, the normal momentum equation was used in order to express the difference between the real and the inviscid static pressures, namely

$$\epsilon P-\epsilon_{\mathrm{e}}P_{\mathrm{e}}=\epsilon\rho\overline{W_{\mathrm{n}}''^2}+\text{h.o.t.} \quad [3]$$

(where h.o.t. denotes higher order terms), which was introduced into the streamwise momentum equation in order to render it in the form of [1]. Equations [1] and [2] are valid for both the axisymmetric case and the case with varying streamtube thickness, by setting the parameter σ equal to the radius R or to the width of the corresponding streamtube, respectively.

The equations can now be developed in their final form. New variables are introduced and certain assumptions are made (Assassa & Papailiou 1979; Papailiou 1970), in order to transform the governing equations to a form suitable for applying the present shear layer calculation method. First, a new form factor L_k is introduced through the relation

$$\mathrm{d}L_k=\frac{\mathrm{d}H_{32k}}{H_{32k}(H_{12k}-1)}. \quad [4]$$

It is worth noting that the l.h.s. of [4] becomes a total differential once the form factor H_{12k} is taken to be a unique function of the form factor H_{32k}. Also that, since the definitions of the form factors H_{12k} and H_{32k}, see [A.9] and [A.11], remain identical in both single- and two-phase flows, the same similarity seems to exist for the form factor L_k. Then, a new intrinsic parameter X defining the shear layer behaviour, is introduced as

$$X=\ln(\mathrm{Re}_3)+2L_k. \quad [5]$$

Finally, the velocity logarithm q and the velocity potential Φ are introduced instead of the velocity W_{Sew} and the arc length s, defined as

$$q=\ln\frac{W_{\mathrm{Sew}}}{W_{\mathrm{ref}}} \quad [6]$$

and

$$\Phi=\int_0^s\frac{W_{\mathrm{Sew}}}{\nu_{\mathrm{ew}}}\mathrm{d}s. \quad [7]$$

By subtracting [1] from [2] and introducing the abovementioned form factors and parameters, the integral momentum equation for the gaseous phase becomes

$$F_1\,\mathrm{d}L_k=F_2\,\mathrm{d}q+\frac{C_{\mathrm{D}}M}{\mathrm{Re}_3}\mathrm{d}\Phi+\frac{F_3}{W_{\mathrm{Sew}}^2}\mathrm{d}\left(\frac{\Omega^2R^2}{2}\right)+\frac{A_{\mathrm{e}}-A_{\mathrm{m}}}{Q}+\frac{G_{\mathrm{e}}-G_{\mathrm{m}}}{Q}, \quad [8]$$

where Q, M, F_1, F_2 and F_3 are quantities, the expressions for which are given in appendix B.

With the introduction of the new form factors and after some rearrangements, the integral energy equation for the gaseous phase takes the form

$$\mathrm{d}X - 2\mathrm{d}L_k = -2\left[1 + (r-\omega)\frac{\gamma-1}{2}M_{\mathrm{ew}}^2\right]\mathrm{d}q + \frac{C_{\mathrm{D}}}{\mathrm{Re}_3}\mathrm{d}\Phi + \frac{(r-\omega)(\gamma-1)M_{\mathrm{ew}}^2}{W_{\mathrm{Sew}}^2}\mathrm{d}\left(\frac{\Omega^2R^2}{2}\right) + A_{\mathrm{e}} + G_{\mathrm{e}}, \quad [9]$$

where ω denotes the constant in Sutherland's law (Papailiou 1981).

The terms G_{m} and G_{e}, expressing the influence of the dispersed phase on the continuous one, have the following form:

$$G_{\mathrm{m}} = \frac{S_{\mathrm{m}}}{\epsilon_{\mathrm{ew}}\rho_{\mathrm{ew}}W_{\mathrm{Sew}}^2}\frac{\mathrm{d}\Phi}{\mathrm{Re}_2} \quad [10a]$$

and

$$G_{\mathrm{e}} = \frac{S_{\mathrm{e}}}{\epsilon_{\mathrm{ew}}\rho_{\mathrm{ew}}W_{\mathrm{Sew}}^3}\frac{\mathrm{d}\Phi}{\mathrm{Re}_3}. \quad [10b]$$

S_{m} and S_{e} stand for terms that embody the momentum and energy exchanges between the two phases as well as between the shear layer and the external flow, in an integral form. Their expressions read

$$S_{\mathrm{m}} = -\int_0^{\delta}[S_{\rho\mathrm{Ws}} - (S_{\rho\mathrm{Ws}})_{n=\delta}]\,\mathrm{d}n + W_{\mathrm{Se}}\int_0^{\delta}[S_\rho - (S_\rho)_{n=\delta}]\,\mathrm{d}n \quad [11]$$

and

$$S_{\mathrm{e}} = -2\int_0^{\delta}W_{\mathrm{S}}[S_{\rho\mathrm{Ws}} - (S_{\rho\mathrm{Ws}})_{n=\delta}]\,\mathrm{d}n + \int_0^{\delta}(W_{\mathrm{S}}^2 + W_{\mathrm{Se}}^2)S_\rho\,\mathrm{d}n - 2\int_0^{\delta}W_{\mathrm{S}}W_{\mathrm{Se}}(S_\rho)_{n=\delta}\,\mathrm{d}n, \quad [12]$$

noting that the mass and momentum source terms, S_ρ and $S_{\rho\mathrm{Ws}}$ respectively, are specified once the calculation of the droplet properties is completed. In addition, $S_{\rho\mathrm{Ws}}$ is defined by

$$S_{\rho\mathrm{Ws}} = \mathbf{S}_{\rho\mathrm{V}} \cdot \mathbf{s}, \quad [13]$$

where $\mathbf{s}$ is the unit vector tangential to the wall and $\mathbf{S}_{\rho\mathrm{V}}$ is the vector of the source terms, representing the momentum exchange between the phases.

2.2. The semi-empirical frame

A basic assumption of the present formulation is that the turbulence semi-empirical frame established for single-phase shear layers is valid for the gaseous phase in two-phase flow problems. A similar statement is made for laminar flow. As an example, for the steam velocity profiles those described by Coles's laws (1955, 1956) are used and the compressibility effects are introduced using the generalized velocity of Van Driest (1951). When the gaseous phase velocity profile is established, the temperature distribution of the carrier phase at a certain station can be calculated using the Crocco relation (Van Driest 1951). Details for the two-dimensional compressible, laminar and turbulent, attached and detached shear layer semi-empirical frame can be found in Papailiou & Bouras (1990) and Papailiou (1981). There, it is explicitly established that two shear layer intrinsic parameters, for instance a form factor and a Reynolds number, are sufficient in order to deduce all the other shear layer properties at a section (local similarity). This is compatible with the two integral equations at hand.

It should be noted that for two-phase flows the semi-empirical relations correlating the gaseous phase kinetic quantities remain unaffected by the presence of the second phase. This is due to the fact that in the definitions of the corresponding thicknesses the void fraction ϵ, which accompanies the gas density, does not appear. In this way, the curves $H_{32k}(H_{12k})$ and $L_k(H_{12k})$, for example, remain identical for the two problems. On the other hand, the development of various semi-empirical relations requires the introduction of the void fraction ϵ or/and the source terms. This

is the case, for instance, for the dissipation factor C_D, which appears in the governing equations and is calculated in a manner similar to the one presented by Papailiou (1981) as

$$C_D = \frac{\left(\frac{u_\tau}{W_{Sew}}\right)^2 H_{32}}{1 + r\frac{\gamma - 1}{2} M_{ew}^2}\left(1 + \frac{\delta_1}{\delta_{1k}}\frac{Q}{H_{12}} F_2 \Pi\right) - \frac{S_e}{\epsilon_{ew}\rho_{ew} W_{Sew}^3}, \qquad [14]$$

where u_τ stands for the friction velocity and Π denotes the shear layer equilibrium parameter, defined as

$$\Pi = \frac{\delta_{1k}}{|\epsilon_w \tau_w|}\frac{d(\epsilon_e P_e)}{ds}.$$

In the same way, appropriate expressions for the two-phase flow case have been developed for the various terms retained in the present formulation. It is worthy of mention that the method is capable of taking into account wall curvature and Coriolis force effects on turbulence (Leoutsakos & Papailiou 1990). Additional corrections for the two-phase case have been made to the terms accounting for the aforementioned influences.

For the correct prediction of flow separation and the subsequent separated region, the normal fluctuation terms, in an integral form, appearing in [8] and [9] are important. As an initial formulation, the single-phase modelling established by Gerolymos *et al.* (1984) is thought to be valid for the two-phase flow as well.

During the shear layer development, an exchange of energy between the two phases is taking place, so that the turbulent shear layer state is influenced by the presence of the liquid phase. The basic assumption that has been made specifies that the general laws established for single-phase turbulent shear flows are valid during this exchange. However, indications exist that turbulent behaviour is affected by the presence of droplets (Mostafa & Mongia 1987). For the moment, in view of the distinct lack of experimental results, it was considered that such an influence is superfluous. However, the formulation of the method is sufficiently flexible that additional information can be easily introduced, when available.

2.3. Lagrangian formulation for the dispersed phase

Two approaches exist for modelling droplet motion throughout the flow field. The first, the "two-fluid" model, treats the dispersed phase as a continuous phase and uses another set of conservation equations, together with appropriate boundary and interface conditions, in order to describe the motion of the dispersed phase. The second, the "trajectory" model, treats the droplets in a Lagrangian fashion; individual droplets are tracked into the flow field and their trajectories, as well as their temperature and diameter histories, are calculated by solving the corresponding transport equations. In this work, the "trajectory" model was selected on the grounds of the advantages it appears to possess over the "two-fluid" model. For a detailed presentation of the relevant advantages and a discussion of the limitations and computer cost of these two models, the reader is referred to the review papers by Mostafa & Mongia (1987) and Crowe (1982).

It is assumed that the droplets are sufficiently dispersed so that droplet–droplet interaction is negligible. This assumption restricts the present study to dilute particulate suspensions. In the discrete droplet approach, the dispersed phase is represented by computational droplets rather than a continuous distribution function. This amounts to a statistical formulation of the problem, since a finite number of droplets is used to represent the very large number of them present in the field. Each of these computational droplets characterizes a group of physical droplets possessing the same characteristic size, velocity and temperature. In the present study, the effect of gas turbulence on droplet dispersion is ignored (deterministic treatment), since turbulent diffusion generally loses its importance in motions of droplets larger than about 3 μm (Menguturk *et al.* 1983).

The entry of the droplets in the flow field is represented by a finite number of entry ports. If $\dot{m}_d$ is the total droplet mass inflow rate, X_j is the mass fraction of droplets entering the field at port

j and Y^k is the mass fraction of droplets with initial diameter d_{in}^k, the number flow rate of spherical droplets having initial diameter d_{in}^k and entering the flowfield at port j is

$$\dot{N}_j^k(d_{in}^k) = \frac{6\dot{m}_d X_j Y^k}{\pi\rho_d (d_{in}^k)^3}. \quad [15]$$

The number flow rate $\dot{N}_j^k$ remains constant along a droplet trajectory (Durst *et al.* 1984).

For large droplet-to-gas density ratios, the only important forces acting on a droplet are the inertia, drag and gravity force, in which case the equation of motion for the kth computational droplet becomes

$$m_d^k \frac{D\mathbf{V}^k}{Dt} = \mathbf{F}_D^k + \left(1 - \frac{\rho}{\rho_d}\right)\mathbf{g} - 2m_d^k(\boldsymbol{\Omega} \times \mathbf{V}^k) - m_d^k[\boldsymbol{\Omega} \times (\boldsymbol{\Omega} \times \mathbf{X}^k)], \quad [16]$$

where $\mathbf{V}$ and $\mathbf{X}$ are the droplet velocity and position vectors, respectively, $\mathbf{F}_D$ is the vector of the drag force, defined as

$$\mathbf{F}_D^k = \frac{1}{2}\frac{\pi(d^k)^2}{4}\rho C_D^k |\mathbf{W} - \mathbf{V}^k|(\mathbf{W} - \mathbf{V}^k), \quad [17]$$

$\mathbf{g}$ is the gravity vector and m_d^k is the mass of the kth computational droplet with diameter d^k. The last two terms in [16] are the Coriolis and centripetal forces, respectively, which appear in the equation of motion when the total derivative D/Dt refers to a coordinate system rotating around the axis of the turbomachine, with a constant angular speed Ω equal to the rotational speed of the machine. In [17], $\mathbf{W}$ denotes the gaseous phase relative velocity vector.

In turbulent flows, the motion of droplets near a solid wall is primarily affected by shear-induced lift, while the effect of the drag increase and the lift caused by free rotation are comparatively small. In this respect, the normal to the wall component of the equation of motion has to be modified by adding the lateral lift term (Saffman 1968), namely

$$F_L = 1.615\mu(d^k)^2\sqrt{\frac{\rho}{\mu}\cdot\frac{\partial W_S}{\partial n}}(W_S - V_S^k), \quad [18]$$

where μ is the dynamic viscosity of the carrier phase. The derivation of [18] was restricted to low droplet Reynolds numbers, which means that it is valid for relatively large shear and small particle sizes. Additionally, [18] was derived for uniform shear (linear velocity gradient), which is almost the case for the region outside the laminar sublayer. In view of these restrictions, the effect of the lift force should be regarded as approximate.

The drag coefficient C_D^k, appearing in [17], is given as a function of the Reynolds number and a correction is added to take into account the mass exchange (Renksizbulut & Haywood 1988):

$$C_D^k = C_{D0}^k(1 + B)^{-0.2}, \quad [19]$$

where B is the transfer coefficient (Spalding number), expressed as

$$B = c_p\frac{T - T_{sat}}{L}, \quad [20]$$

where c_p, T, T_{sat} and L denote the gaseous phase specific heat at constant pressure, temperature, saturation temperature and latent heat of vaporization, respectively, and

$$C_{D0}^k = \begin{cases} 24/\mathrm{Re}_d^k, & \mathrm{Re}_d^k < 1 \\ 24/\mathrm{Re}_d^k[1 + 0.15(\mathrm{Re}_d^k)^{0.687}], & 1 \leqslant \mathrm{Re}_d^k \leqslant 1000 \\ 0.44, & \mathrm{Re}_d^k > 1000; \end{cases} \quad [21]$$

with the droplet Reynolds number defined as

$$\mathrm{Re}_d^k = \frac{\rho|\mathbf{W} - \mathbf{V}^k|d^k}{\mu}. \quad [22]$$

The droplet location at any instant of time is determined from

$$\frac{D\mathbf{X}^k}{Dt} = \mathbf{V}^k. \quad [23]$$

The mass equation for the kth computational droplet yields

$$\frac{Dm_d^k}{Dt} = \dot{m}_d^k = -\frac{\rho_d(\pi k)d^k}{\rho c_p} \cdot \ln(1+B)[2 + 0.56(\mathrm{Re}_d^k)^{0.5}(\mathrm{Pr})^{0.33}], \quad [24]$$

where $m_d^k = \rho_d \pi (d^k)^3/6$ and the term in the brackets expresses a correction factor (=Nu) used to model the vaporization rate in a convective field (Crowe *et al.* 1977), while Pr stands for the Prandtl number of the carrier phase. The heat balance equation for the droplet reads

$$m_d^k c_d \frac{DT_d^k}{Dt} = \mathrm{Nu}(\pi k)d^k(T - T_d^k) + L\left(\frac{Dm_d^k}{Dt}\right), \quad [25]$$

where c_d is the specific heat of droplet and k is the thermal conductivity of the carrier phase. The first r.h.s. term of the above equation expresses the heat absorbed from the surrounding gas by convection only, while the second term is the heat due to evaporation.

When droplet properties are known in each node of a certain cross-section, the carrier phase mass and momentum source terms per unit volume, resulting from all particle trajectories, are obtained as follows:

$$S_\rho = \sum_{k=1}^{\mathrm{NID}} [N^k \dot{m}_d^k] \quad [26]$$

and

$$\mathbf{S}_{\rho V} = -\sum_{k=1}^{\mathrm{NID}} [N^k(\mathbf{F}_D + \dot{m}_d \mathbf{V})^k], \quad [27]$$

and the void fraction ϵ as

$$\epsilon = 1 - \sum_{k=1}^{\mathrm{NID}} \left[N^k \frac{\pi(d^k)^3}{6} \right], \quad [28]$$

where NID stands for the number of the initial droplet diameters and N^k stands for the number density of droplets with initial diameter d_{in}^k. The number density N^k is related to the number flow rate $\dot{N}^k$ as follows:

$$\dot{N}^k = N^k |\mathbf{V}^k|. \quad [29]$$

2.4. The solution procedure

The integral shear layer method requires the knowledge of the flow quantities distributions along the solid walls; these are obtained from the solution of the inviscid flow solver. In a two-phase flow problem, besides the gaseous phase external flow velocity distribution, the droplets' properties (diameter, velocity components etc.) are also required at the edge of the shear layer. This information determines whether droplets flow in or out of the shear layer domain, as the calculation marches downstream. The inlet velocity and temperature profiles need to be specified also. The wall's orientation with respect to the rotating axis is necessary in order to evaluate the second-order terms appearing in the equations and the influence of the Coriolis force and streamline curvature on turbulence.

Considering two successive streamwise positions inside the shear layer, one where all the flow quantities are known and the following one, where the quantities have to be calculated, the procedure starts by assuming a steam velocity profile at the second (current) location. In this manner, an approximate flow field is established. Then, a trajectory calculation is performed in the interval between the two considered positions and the liquid phase flow field at the current station is thus obtained. Equations [8] and [9] are solved in turn for the gaseous phase with updated source terms, using a Newton–Raphson method. A new steam velocity profile can now be determined and the procedure continues until convergence.

For the trajectory calculation, a classical geometrical transformation is employed, which maps the real flow domain (x, y) to a computational one (ξ, η) with equidistant nodes. A fourth-order Runge–Kutta scheme is used to transfer information from a certain cross-section to the next, where droplet properties have to be calculated, except from the point at the wall.

For the present investigation it is assumed that when the droplets reach the wall surface they remain on the wall, slipping over it. This assumption is quite a realistic one and becomes more

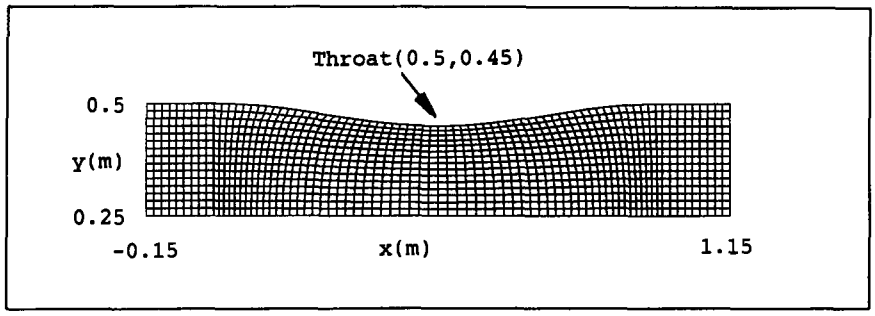

Figure 2. Geometry and mesh of the upper half of the duct

convenient in the case where a liquid film flows underneath the core shear layer. So, the boundary conditions for the dispersed phase are:

$$V_n^k = 0, \quad \frac{\partial V_S^k}{\partial n} = 0, \quad \frac{\partial N^k}{\partial n} = 0.$$

3. RESULTS AND DISCUSSION

Numerical solutions were obtained for two-dimensional compressible flows passing through a rectangular convergent–divergent duct, shown in figure 2. The distributions of the external flow quantities along the upper and lower walls, necessary for the prediction of the shear layer development along these surfaces, were obtained from the two-phase Euler code presented by Malamatenios *et al.* (1990).

To establish a baseline for two-phase flow modelling, predictions of a single-phase fluid flow field were made first (case 0). Then, two mass loading ratios, defined as the ratio of droplet-to-gas mass flow rate at the inlet plane, LR = 1 and LR = 2, were considered for droplets with initial diameter $d_{in} = 10\ \mu$m (cases 1 and 2); while for the droplets with $d_{in} = 5\ \mu$m, LR = 1 (case 3). Test runs were performed for an isentropic Mach number of the external steam flow equal to 0.3. Figure 3 presents the calculated distribution of the inviscid steam velocity along the lower wall for cases 0 and 2.

The inlet conditions for the shear layer calculations were $\mathrm{Re}_\delta = 75{,}000$ and $u_\tau / W_{Se} = 0.035$. Steam was treated as a perfect gas with isentropic exponent $\gamma = 1.33$. The saturation temperature T_{sat} has been calculated from the steam static pressure P using the relation

$$T_{sat}(\mathrm{K}) = 45. + 1668.21/[10.09171 - \log_{10}(P)].$$

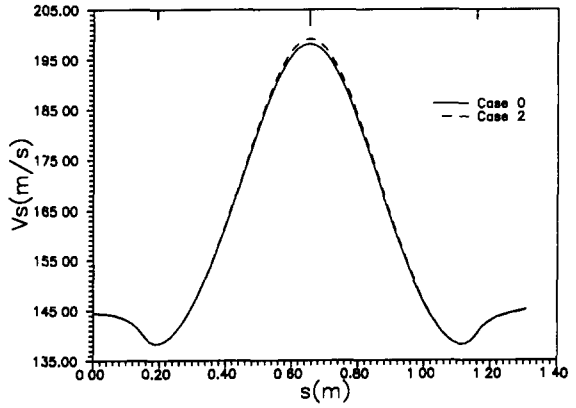

Figure 3. Gaseous phase inviscid velocity distributions along the lower wall of the duct. (The three ticks on the upper border of the figure stand for the end of the upstream straight part, the throat and the start of the downstream straight part, respectively.)

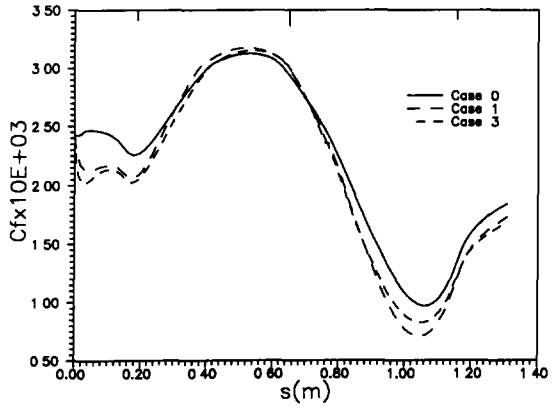

Figure 4. Skin friction coefficient distribution along the lower surface for various droplet sizes (LR = 1).

The initial droplet density profile at the inlet of the shear layer was assumed to follow a second-order distribution across the section and the inlet droplet velocity was equal to that of the gaseous phase.

Figures 4 and 5 present the skin friction coefficient C_f distribution along the lower surface, for the four cases. From its definition, [A.13], it can be seen that the skin friction coefficient may be calculated once the gaseous phase velocity profile is established. The first figure is used to compare cases with the same LR but different initial droplet diameters and the second one to examine the flow behaviour for different LR values, for the same initial droplet diameter. Apart from a small region in the convergent part of the duct, C_f is smaller in a two-phase than in a single-phase environment. For the same LR, the smaller the droplets are the smaller the friction coefficient is, at least out of abruptly accelerating or decelerating flow regions (figure 4). This can be explained by the fact that, for the same loading, the effective droplet area increases when the droplet size falls and hence, the rate of exchange of mass, momentum and energy increases as well. This reduction of C_f becomes more pronounced in the case where droplets double their population (figure 5).

In the convergent part of the duct, droplets hit the solid wall and this results in a local increase in the C_f values. On the other hand, downstream of the throat, where the flow tends to recover, the droplets move almost parallel to the wall and a significant reduction of C_f is observed. Such a reduction has also been observed by Pfeffer & Kane (1976), who claimed that this behaviour is due to the reduction of the gas viscosity, the thickening of the laminar sublayer and/or general turbulence suppression. In the present analysis, no important temperature difference in the steam was observed between the single- and two-phase flow cases which would result in a reduction of the steam viscosity. On the other hand, the authors believe that, with respect to the present model, the explanation must be traced to the increase in the dissipation factor C_D. Its streamwise distribution is presented in figure 6. The turbulent energy dissipation, being higher for the gaseous phase when droplets are present, demonstrates that the shear layer is closer to separation. It is expected, then, for the corresponding skin friction values to be closer to zero.

Figure 7 presents the form factor H_{12} distribution along the lower surface for all four cases. It is observed that strong similarities exist in the four H_{12} distributions, all exhibiting an opposite trend to that of C_f. Finally, the distribution of the energy thickness is presented in figure 8, for all the test cases and for the lower wall surface. This quantity corresponds to the mean kinetic energy loss having occurred in the shear layer with respect to the external flow at the same station. It is observed that during the acceleration phase, the loss occurring in the shear layer with respect to what has occurred in the outer flow, is almost identical for all cases. During the deceleration phase, however, the loss increases for the two-phase situation. The loss is highly influenced by the LR and increases with increasing loading.

Similar behaviour has been observed for the distributions calculated for the upper surface, where slight differences between the corresponding curves are attributed to the gravity effects on droplet motion.

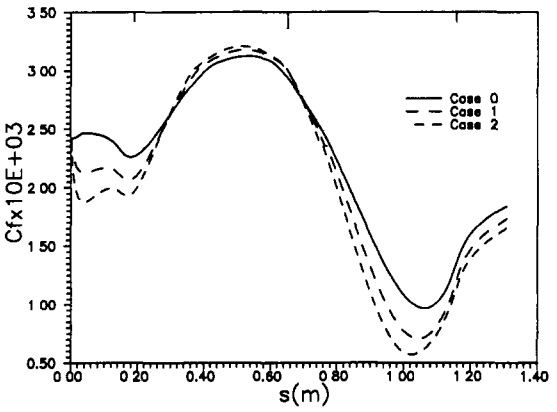

Figure 5. Skin friction coefficient distribution along the lower surface for various droplet loading ratios ($d_{in} = 10\,\mu$m).

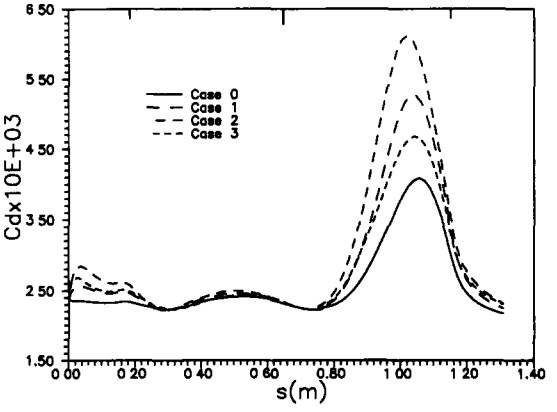

Figure 6. Effect of droplet presence on the steam dissipation factor C_D.

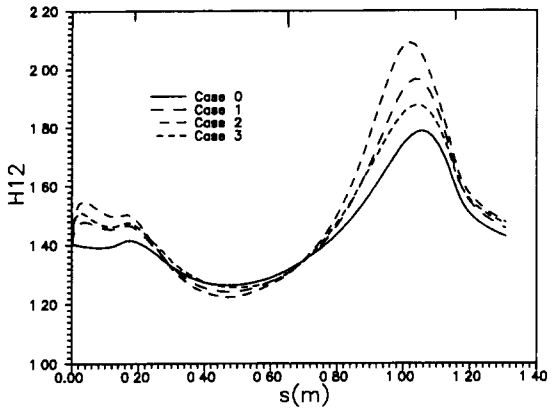

Figure 7. Effect of droplet presence on the form factor H_{12}.

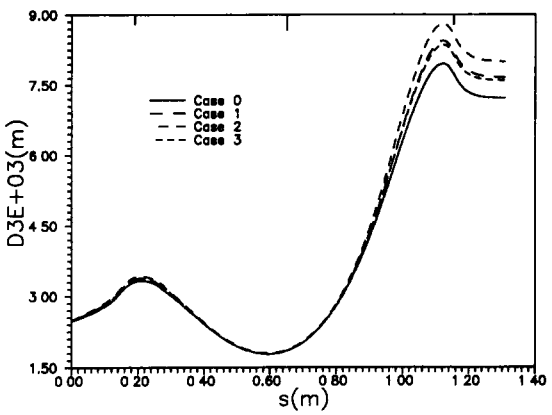

Figure 8. Effect of droplet presence on the steam energy thickness.

4. CONCLUSIONS

A two-phase shear layer calculation procedure was presented, capable of predicting the non-equilibrium effects in the vicinity of blade surfaces of wet steam turbines. The method provides information on the development of the steam shear layer along the blade surface and the motion of the droplets within the shear layer. The computational time is quite reasonable.

Test runs were performed for the lower and upper surfaces of a two-dimensional convergent–divergent duct and qualitative comparisons are presented along with single-phase results. A reduction of the skin friction coefficient was observed in the two-phase case in regions where droplets move parallel to the wall. This was attributed to the corresponding increase in the dissipation factor values. On the other hand, the H_{12} and δ_3 distributions were found to have a rather similar behaviour in single- and two-phase flows. Differences between the upper and lower wall distributions were attributed to gravity effects. Unfortunately, a detailed quantitative validation of the method could not be realized due to the lack of available experimental data for comparison.

The authors believe that the above calculations shed some light on the nature of the viscous phenomena occurring in wet steam flows and that it will eventually be possible to supply the turbine designer with a reliable computational tool.

Acknowledgements—Part of the work presented herein was carried out in the context of the BRITE Project P-2156, entitled "The study of non-equilibrium two-phase flow in steam turbines". The authors are indebted to Mr V. Bouras for supplying his experience on the development and use of integral shear layer methods for single-phase flow problems.

REFERENCES

ASSASSA, M. G. & PAPAILIOU, K. D. 1979 An integral method for calculating the turbulent boundary layer with separation. *J. Fluids Engng* **100**, 110–116.

BOURAS, V. 1991 Integral method for the calculation and optimization of laminar and turbulent shear layers in the presence of flow separation. Ph.D. Thesis, N.T.U.A., Greece. In preparation.

COLES, D. 1955 The law of the wake in the turbulent boundary layer. Guggenheim Aero. Lab., Caltech, Pasadena, CA.

COLES, D. 1956 *The Law of the Wall in Turbulent Shear Flow 50 Jahre Grenzschicht Forschung*. Vieweg, Braunsweig.

CROWE, C. T. 1982 REVIEW—numerical models for dilute gas–particle flows. *J. Fluids Engng* **104**, 297–303.

CROWE, C. T., SHARMA, M. P. & STOCK, D. E. 1977 The particle-source-in cell (PSI-CELL) model for gas–droplet flows. *J. Fluids Engng* **99**, 325–332.

DELHAYE, J. M. 1981 Local time-averaged equations. In *Thermohydraulics of Two-phase Systems for Industrial Design and Nuclear Engineering* (Edited by DELHAYE, J. M., GIOT, M. & RIETHMULLER, M. L.), pp. 171–178. Hemisphere, McGraw-Hill.

DURST, F., MILOJEVIC, D. & SCHONUNG, B. 1984 Eulerian and Lagrangian predictions of particulate two-phase flows: a numerical study. *Appl. Math. Modeling* **8,** 101–115.

GEROLYMOS, G., KALLAS, Y. & PAPAILIOU, K. D. 1984 The behaviour of the normal fluctuation terms in the case of attached and detached turbulent boundary layers. ASME Paper 84-GT-179.

LEOUTSAKOS, G. & PAPAILIOU, K. D. 1990 Curvature and Coriolis correction on the dissipation factor C_D for turbulent boundary layers (unseparated and separated). Thermal Turbomachines Lab., Internal Report.

MALAMATENIOS, CH., GIANNAKOGLOU, K. & PAPAILIOU, K. D. 1990 A calculation method for gas–droplet flows in turbomachinery components including viscous effects. Paper presented at the *Int. Symp. on Engineering Turbulence and Measurements*, Dubrovnik.

MENGUTURK, M., GUNES, D., MIMAROGLU, H. K. & SVERDRUP, E. F. 1983 Blade boundary layer effect on turbine erosion and deposition. *J. Fluids Engng* **105,** 270–276.

MOSTAFA, A. A. & MONGIA, H. C. 1987 On the modeling of turbulent evaporating sprays: Eulerian versus Lagrangian approach. *Int. J. Heat Mass Transfer* **30,** 2583–2593.

PAPAILIOU, K. D. 1970 Boundary layer optimization for the design of high turbine axial flow compressor blades. ASME Paper 70-GT-88.

PAPAILIOU, K. D. 1981 Le Foll's method and the calculation of attached and separated two-dimensional boundary layers. *Von Karman Institute Lecture Series on Separated Flows in Turbomachinery Components*, VKI LS 1981-1.

PAPAILIOU, K. D. & BOURAS, V. 1990 Arbitrary blade section design based on viscous considerations. *Von Karman Institute Lecture Series on Inverse Methods in Airfoil Design for Aeronautical and Turbomachinery Applications*, VKI LS-90 PR-90 05.

PFEFFER, R. & KANE, R. S. 1976 A review of drag reduction in dilute gas–solid suspension flow in tubes. Presented at the *Int. Conf. on Drag Reduction*, Cambridge.

RENKSIZBULUT, M. & HAYWOOD, R. J. 1988 Transient droplet evaporation with variable properties and internal circulation at intermediate Reynolds numbers. *Int. J. Multiphase Flow* **14,** 189–202.

SAFFMAN, P. G. 1968 Corrigendum to "The lift of a small sphere in a slow-shear flow". *J. Fluid Mech.* **31,** 624.

VAN DRIEST, E. R. 1951 Turbulent boundary layers in compressible Fluids. *J. Aero Sci.* **18.**

APPENDIX A

The various characteristic quantities of the shear layer, as modified for the two-phase flow case, are defined as follows:

displacement thickness δ_1,

$$\epsilon_{ew}\rho_{ew}W_{Sew}\delta_1 = \int_0^\delta (\epsilon_e\rho_e W_{Se} - \epsilon\rho W_S)\,dn; \qquad [A.1]$$

momentum thickness δ_2,

$$\epsilon_{ew}\rho_{ew}W_{Sew}^2\delta_2 = \int_0^\delta (W_{Se} - W_S)\epsilon\rho W_S\,dn; \qquad [A.2]$$

energy thickness δ_3,

$$\epsilon_{ew}\rho_{ew}W_{Sew}^3\delta_3 = \int_0^\delta (W_{Se}^2 - W_S^2)\epsilon\rho W_S\,dn; \qquad [A.3]$$

kinetic displacement thickness δ_{1k},

$$W_{Sew}\delta_{1k} = \int_0^\delta (W_{Se} - W_S)\,dn; \qquad [A.4]$$

kinetic momentum thickness δ_{2k},

$$W_{Sew}^2 \delta_{2k} = \int_0^\delta (W_{Se} - W_S) W_S \, dn; \qquad [A.5]$$

kinetic energy thickness δ_{3k},

$$W_{Sew}^3 \delta_{3k} = \int_0^\delta (W_{Se}^2 - W_S^2) W_S \, dn; \qquad [A.6]$$

and

density thickness δ_ρ,

$$\epsilon_{ew} \rho_{ew} \delta_\rho = \int_0^\delta (\epsilon_e \rho_e - \epsilon \rho) \, dn, \qquad [A.7]$$

where ϵ, ρ, δ and W_S denote the gaseous phase residence time fraction, material density, boundary layer thickness and relative velocity tangent to the wall, respectively. Subscripts e and w stand for external flow quantities and values at the wall, respectively.

According to the previous definitions, the momentum thickness form factors H_{12} and H_{12k}, the energy form factors H_{32} and H_{32k} and the density form factor $H_{\rho 2}$ are given by

$$H_{12} = \delta_1 / \delta_2, \qquad [A.8]$$

$$H_{12k} = \delta_{1k} / \delta_{2k}, \qquad [A.9]$$

$$H_{32} = \delta_3 / \delta_2, \qquad [A.10]$$

$$H_{32k} = \delta_{3k} / \delta_{2k} \qquad [A.11]$$

and

$$H_{\rho 2} = \delta_\rho / \delta_2. \qquad [A.12]$$

The skin friction coefficient C_f is defined as

$$C_f = \frac{2 \epsilon_w \tau_w}{\epsilon_{ew} \rho_{ew} W_{Sew}^2} = 2 \frac{\epsilon_w \rho_w}{\epsilon_{ew} \rho_{ew}} \cdot \left(\frac{u_\tau}{W_{Sew}} \right)^2, \qquad [A.13]$$

where τ_w stands for the wall shear stress.

The dissipation factor C_D is given by

$$C_D = \frac{2}{\epsilon_{ew} \rho_{ew} W_{Sew}^3} \int_0^\delta \epsilon \tau \frac{\partial W_S}{\partial n} \, dn. \qquad [A.14]$$

The Reynolds numbers Re_i, based on various thicknesses δ_i, are defined by

$$Re_i = \frac{W_{Sew} \delta_i}{\nu_{ew}}, \qquad [A.15]$$

where ν is the kinematic viscosity of the gaseous phase.

APPENDIX B

This appendix gives the expressions of the quantities appearing in [8]; it is worth noting that they are identical to the corresponding coefficients of the single-phase flow equations, given in detail by Papailiou & Bouras (1990):

$$Q = (H_{12} - 1) - r(\gamma - 1) M_{ew}^2, \qquad [B.1]$$

$$M = [1 - C_f H_{32} / (2 C_D)] / Q, \qquad [B.2]$$

$$F_1 = (H_{12k} - 1) / Q, \qquad [B.3]$$

$$F_2 = \frac{[1 + (\gamma - 1)M_{ew}^2/2](2K_1 M_{ew} + 3K_2 M_{ew}^2)M_{ew}}{Q \cdot (1 + K_1 M_{ew}^2 + K_2 M_{ew}^3)} \quad [B.4]$$

and

$$F_3 = [r(\gamma - 1)M_{ew}^2 - H_{\rho 2}]/Q. \quad [B.5]$$

The constants K_1 and K_2 appearing in [B.4], result from the use of the relation

$$H_{32} = H_{32k}(1 + K_1 M_{ew}^2 + K_2 M_{ew}^3) \quad [B.6]$$

in the derivation of the final form of the gaseous phase integral momentum equation. Relation [B.6] connects the form factor H_{32} with the kinetic form factor H_{32k} and the Mach number of the external flow and is valid for unseparated gaseous phase shear layers, according to Papailiou (1981).